Progress In Electromagnetics Research C, Vol. 110, 119–133, 2021

Metasurface Superstrate Inspired Printed Monopole Antenna for RF Energy Harvesting Application

Bikash R. Behera, Priya R. Meher, and Sanjeev K. Mishra*

Abstract—In this paper, a metasurface superstrate-inspired broadband circularly polarized (CP) printed monopole antenna is investigated. To achieve broadband circular polarization and directional radiation pattern, a circle-shaped monopole radiator with asymmetrical staircased partial ground loaded with metasurface is introduced. It is fed by a 50-Ω microstrip feedline and is fabricated on an FR-4 substrate, having overall dimension of $1.25\lambda_0 \times 1.66\lambda_0 \times 0.02\lambda_0$ at $f = 5$ GHz. The metasurface antenna exhibits a measured impedance bandwidth of 5 GHz (1.85–6.85 GHz, 114.9%), axial bandwidth of 910 MHz (4.09–5 GHz, 20.02%) with average CP antenna gain of 6.82 dBic, directional radiation pattern and consistent antenna efficiency of $> 85.65\%$ in the desired frequency bands. Time domain characteristics, i.e., group delay is obtained within 2 ns in the operating frequency bands. Due to its design process and attainment of broadband CP, higher antenna gain, and directional radiation pattern in the broadside direction, it is extended for RF energy harvesting. The proposed metasurface antenna is integrated with a rectifier circuit, where RF-to-DC conversion efficiency (η_0) and DC output voltage (V_{out}) are analyzed by using ADS circuit solver.

1. INTRODUCTION

With the rapid growth of modern RF applications in sub-6 GHz bands, there is a requirement of RF front-ends operating in the electromagnetic spectrum of RFID, GPS, 3G, UMTS (2.1 GHz), LTE (2.6 GHz), LTE (3.5 GHz), Wi-Fi (2.4/5 GHz), WiMAX (2.5/3.5/5.5 GHz), ISM (2.4/5 GHz), 5G (5 GHz), and WLAN (IEEE 802.11 b/g/n). Due to the presence of such type of ambient RF signals in the environment, they are often considered as the intrinsic part of RF energy harvesting system and other wireless communication platforms [1]. In this scenario, their effectiveness is visualized with the features of circular polarization (CP). It is quite essential, due to the advantages like reduced multi-path interference and better signal matching, ensuring that signals are properly received irrespective of the orientation of antenna [2, 3]. In our study, a printed monopole antennas is chosen due to its low-profile characteristics, low cost, reasonable antenna efficiency, omnidirectional radiation pattern over the entire frequency bands, good time domain performance, and easy analysis. For this reason, it has been considered as an asset for the operation in UWB (3.1–10.6 GHz) [4, 5]. However, its implementation in the 1-to-7 GHz spectrum is limited in number [6].

In [7–10], although the monopole antenna operates in the required spectrum, non-existence of CP fails to support their viability from applications point of view. In the reported instances of [11–19], CP is achieved due to the change in antenna geometry [11], incorporation of metasurfaces/artificial magnetic conductors (AMCs) [12–15], addition of slots [16, 17], introduction of fractals [18], and modification in feeding mechanism [19]. In [11], a rectangle-shaped monopole antenna is investigated for CDMA and GSM bands with axial bandwidth within 5% in their respective bands. When the antenna structure is embedded with metasurfaces or AMCs [12–15] as a reflector/superstrate, obtained axial bandwidths of

Received 14 January 2021, Accepted 10 February 2021, Scheduled 22 February 2021
* Corresponding author: Sanjeev Kumar Mishra (sanjeev@iiit-bh.ac.in).
The authors are with the Advanced RF and Microwave Lab, International Institute of Information Technology, Bhubaneswar, Odisha 751003, India.

10% in [12], 18.5% [13], 18.69% [14], and 18% [15] are reported. In current scenario, their main objective is to enhance the performance of axial bandwidth, antenna directivity, and antenna gain, along with the attainment of directional radiation properties with wide 3-dB angular beamwidth over the CP bands.

To further investigate CP attributes, a number of cases of dielectric resonator antennas (DRAs) [16–19] have been discussed. In [16], a stair-shaped DR excited by a coupled slot is investigated with the axial bandwidth of 10.6%. To widen the 3-dB axial bandwidth, a rotated-stair DR excited by a slot is presented with CP bandwidth of 18.2% [17]. The fractal concept is soon introduced for improving the axial bandwidth, but it remains limited to 14.01% [18]. Hence, a new dual-mode CP DRA with low-profile nature with axial bandwidth of 17.59% is reported. Although polarization agility was witnessed in [16–19], the overall complexity of structure also increased. Besides, none of the referred papers [7–19] provided any approach towards the investigation of theoretical insights about the attainment of CP mechanism.

Here, a metasurface superstrate-based broadband CP monopole antenna is proposed. The broadband traits of CP and directional radiation pattern in broadside direction are achieved by using an asymmetrical staircased partial ground plane and the incorporation of metasurface as a superstrate. The asymmetrical staircased ground plane is responsible for the generation of both horizontal and vertical field components to achieve circular polarization. With the incorporation of metasurface superstrate, the antenna offers enhancement in 3-dB axial bandwidth, antenna directivity, antenna gain and helps in maintaining consistent antenna efficiency in the desired frequency bands. Besides simulation and characterization, a detailed analogy is backed by the interpretation of surface current distribution, electric-field pattern, along with the theoretical context of plane-waves and far-field normalized radiation pattern. The prospective outcomes offer physical insights of designing RF front-end with broadband CP and directional pattern, a basic requirement for RF energy harvesting [1, 20, 21]. These developments are in general compensated, in the theoretical context, by time domain analysis and implementing the proposed multi-stage rectifier circuit embedded with metasurface antenna within the operating regions of Wi-Fi (2.4/5 GHz), Wi-MAX (2.5/3.5/5 GHz), ISM (2.4/5 GHz) and 5G (5 GHz). Table 1 compares the performance index of proposed metasurface antenna with existing ones [7–19], operating in the bandwidth of 1-to-7 GHz.

Table 1. A comparison of measured metrics between proposed antenna with existing antenna designs reported in [7–19]. [Trade-offs considered for the analysis like (a) impedance and axial bandwidth with fractional bandwidth of $\geq 20\%$, (b) CP antenna gain of > 6.5 dBic and (c) antenna efficiency of $> 85\%$ in the desired operating bands].

Ref.	Antenna	Impedance Bandwidth	Axial Bandwidth	CP Antenna Gain	Antenna Efficiency	Time Domain Analysis
[7]	Monopole	167%	———	———	$> 70\%$	———
[8]	Monopole	154%	———	———	$> 70\%$	———
[9]	Monopole	152%	———	———	$> 70\%$	———
[10]	Monopole	175%	———	———	$> 70\%$	———
[11]	Monopole	CDMA + GSM	$< 5.1\%$	3.5–4.1 dBic	$> 70\%$	———
[12]	Monopole	16%	10%	5.5 dBic	$> 80\%$	———
[13]	Monopole	33.7%	16.5%	5.8 dBic	$> 80\%$	———
[14]	Monopole	34.3%	18.69%	5.1 dBic	$> 80\%$	———
[15]	Dipole	16.8%	18%	< 4.8 dBic	$> 75\%$	———
[16]	DRA	36.6%	10.6%	———	$> 85\%$	———
[17]	DRA	31%	18.2%	4–4.5 dBic	$> 85\%$	———
[18]	DRA	35.59%	14.01%	2.68 dBic	$> 85\%$	———
[19]	DRA	26.84%	17.59%	3.86 dBic	$> 85\%$	———
Proposed	Monopole	114.9%	20.02%	6.82 dBic	$> 85.65\%$	Investigated

2. ANTENNA DESIGN

2.1. Proposed Antenna Configuration

The schematic geometry of the proposed printed monopole antenna loaded with metasurface is shown in Figure 1. It is fabricated on an FR-4 substrate ($\varepsilon_r = 4.4$, $\tan\delta = 0.018$) with overall dimension of $1.25\lambda_0 \times 1.66\lambda_0 \times 0.02\lambda_0$, where λ_0 is considered as the free guided wavelength at $f = 5\,\text{GHz}$. The evolution of this antenna involves three stages. At stage-1, a $\lambda/4$ linearly polarized (LP) circularly-shaped monopole antenna with partial ground plane is designed (initial). At stage-2, the conventional partial ground plane is modified into an asymmetrical staircased partial ground plane, which leads to exciting both horizontal (x) and vertical (y) field components, required for generation of CP waves. Finally, at stage-3, the metasurface as a superstrate is placed just on the top of monopole radiator at a height of $0.75\lambda_0$, supported by the plastic spacers. It leads to the achievement of broadband CP, higher gain, and directional radiation pattern with wide 3-dB angular beamwidth. A detailed analogy about them is presented in Subsections 2.2–2.4, along with their outcomes shown in Figures 2–5. CST microwave studio as a EM solver is used for the design, optimization, and realization of proposed antenna configurations (stage-1 to stage-3).

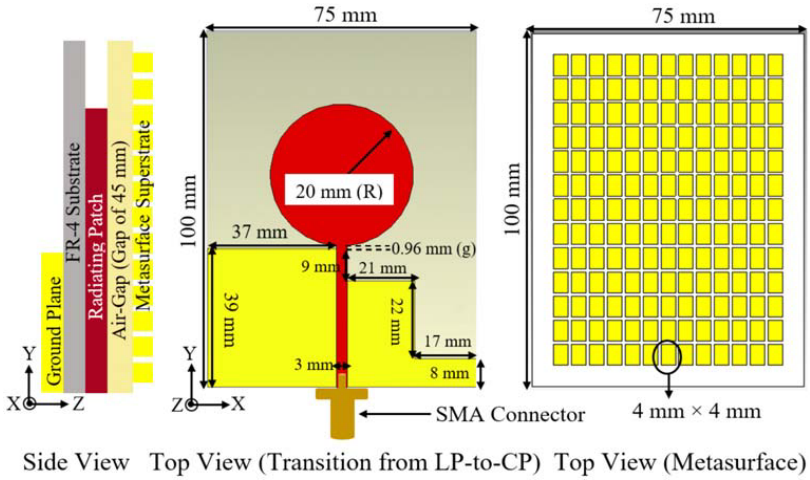

Figure 1. Schematic configuration of the proposed metasurface antenna.

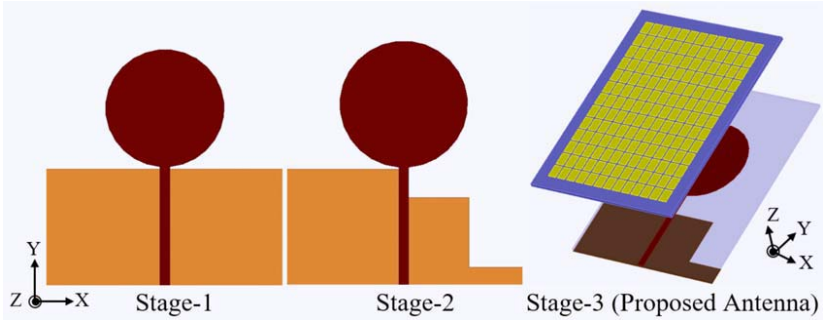

Figure 2. Evolution stages, i.e., stage-1 (initial) to stage-3 (final) of the proposed metasurface antenna.

2.2. Design Process of Stage-1

The dimension of the proposed antenna can be derived using Equation (1).

$$f_L = \frac{7.2}{2.34R + g} \tag{1}$$

where f_L is the lowest resonant frequency, R the radius of the structure, and g the gap between radiating patch and ground plane, which helps in improving the impedance matching of antenna [4]. $f_L = 1$ GHz is considered for the design of circular monopole antenna (CMA) and obtained simulated impedance bandwidth from 1.2 to 7.2 GHz and average LP antenna gain of 3.4 dBi.

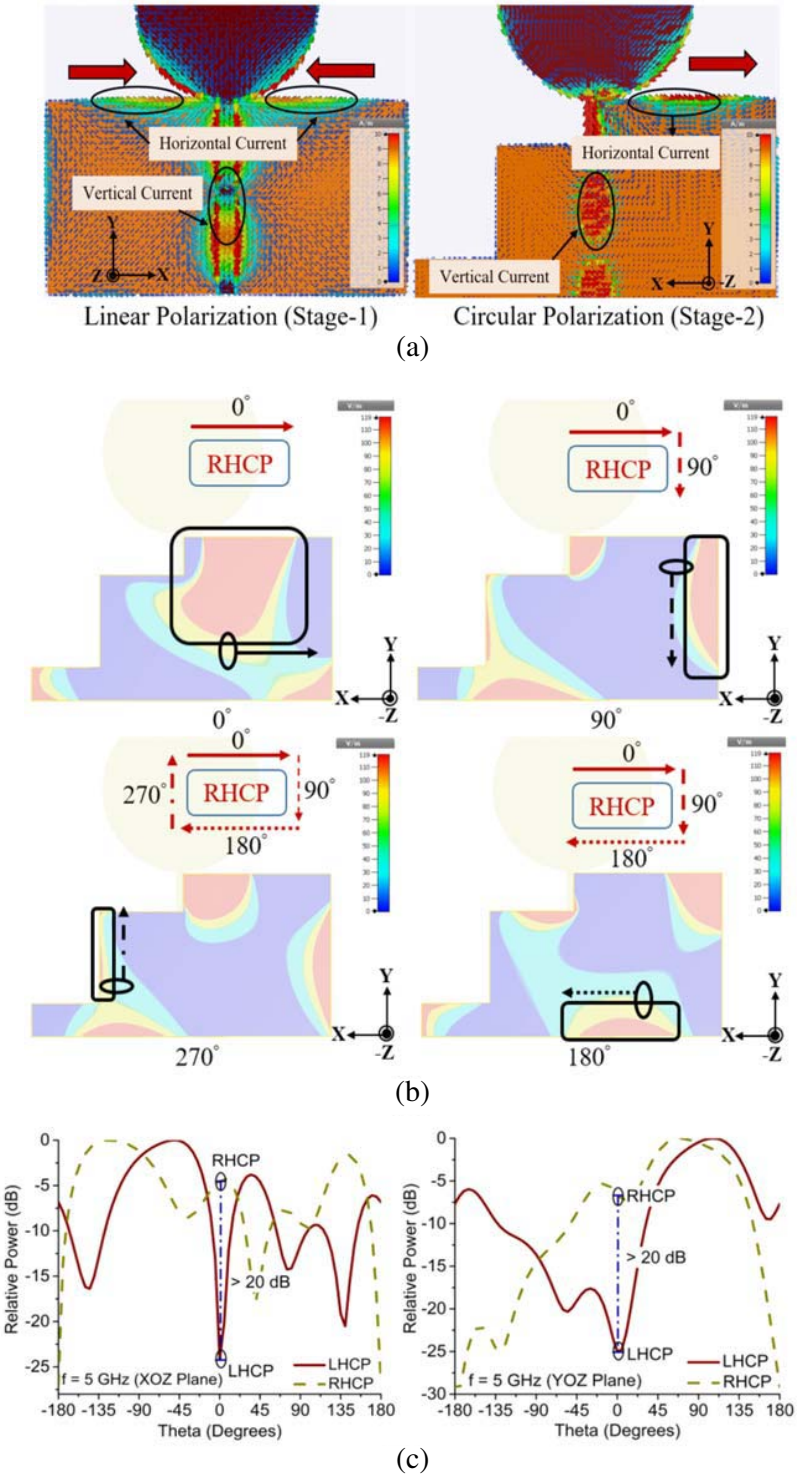

Figure 3. The analysis of CP mechanism at $f = 5$ GHz, (a) surface current distribution [1st approach], (b) electric field distribution [2nd approach] and (c) normalized radiation pattern [3rd approach].

2.3. Design Process of Stage-2

Due to the modification of partial ground plane into asymmetrical staircased partial ground plane in stage-2, horizontal (x) and vertical (y) field components are generated. Here, broad impedance bandwidth from 1.1 to 6.8 GHz, wide axial bandwidth from 4.65 to 5.37 GHz, and average CP antenna gain of 2.3 dBic are achieved. For analyzing the CP characteristics, three different approaches are discussed, as shown in Figures 3(a)–(c).

In the 1st approach, CP behaviour is analyzed using the surface current distribution phenomenon. In stage-1, surface currents cancel at the horizontal edges of partial ground plane, i.e., oppositely directed, which indicates the presence of only vertical currents at the monopole arm. As a result, linearly polarized radiated wave is generated. In stage-2, due to the asymmetrical staircased partial ground plane, horizontal currents exist at horizontal edges of partial ground plane, whereas vertical currents are already present at the monopole arm. The presence of both horizontal and vertical currents confirms the generation of circularly polarized radiated wave [19, 22], as shown in Figure 3(a).

In the 2nd approach, CP behaviour is analyzed using the electric field distribution phenomenon. The nature of CP depends upon the orientation of electric fields, which moves in the clockwise (CW) direction, along with direction of propagation, i.e., $-z$-axis. It is observed that the two field components horizontal (x) and vertical (y) components rotate with 90° phase. Such trends are observed in Figure 3(b), when the maximum magnitude of electric fields orients in clockwise direction. This development is characterized by right-hand thumb rule and visualized through the concept of plane wave equations. A generalized equation [23] is shown below, which interprets the behaviour of electric field pattern shown in Figure 3(b).

$$\overrightarrow{E}_{\mathrm{RHCP}}(z,t) = E_0\cos(\omega t + \beta z)\hat{x} + E_0\cos(\omega t + \beta z + 90^\circ)\hat{y} \tag{2}$$

Putting $z = 0$ in above equation, the final expression for electric fields of RHCP becomes

$$\overrightarrow{E}_{\mathrm{RHCP}}(0,t) = E_0\cos(\omega t)\hat{x} + E_0\cos(\omega t + 90^\circ)\hat{y} \tag{3}$$

In the 3rd approach, CP behaviour is analyzed using the relative power from normalized radiation pattern phenomenon. From Figure 3(c), it is observed that RHCP is stronger than LHCP by more than -20 dB at $f = 5$ GHz, which confirms that the proposed antenna is an RHCP antenna. The dominance of CP components is computed by using a CP relationship given in [2]. Therefore, a summary is drawn that 1st approach relates with existence of CP, whereas 2nd and 3rd approaches relate with finding the nature of CP for the proposed antenna design. The above analysis of evaluating circular polarization characteristics can be even extended to other CP antennas, irrespective of its antenna geometry and frequency of operation [22].

2.4. Design Process of Stage-3

In this stage, prerequisites such as broadband circular polarization (CP), higher antenna gain, consistent antenna efficiency, and directional radiation pattern are attained [21]. The incorporation of a metasurface superstrate at a height of $0.75\lambda_0$ above circularly-shaped radiator is designed to achieve enhancement in antenna performance. The proposed rectangular metasurface, with a surface area of $1.05\lambda_0 \times 1.46\lambda_0$ used as a superstrate, consists of grid-slotted sub-patches of 13×13 cells, where each cell is of $0.06\lambda_0 \times 0.1\lambda_0$ with an intermediate gap of $0.015\lambda_0$. The existence of higher order modes correlates to the achievement of broad impedance and axial bandwidth [24].

When the metasurface superstrate comes in contact with circularly-shaped radiator, it redirects one-half of the radiated waves to the opposite direction and improves the antenna gain (a rise of 2.94 times, i.e., 2.3 dBic to 6.78 dBic). Therefore, the radiated wave from superstrate-loaded antenna includes the wave directed from circularly-shaped radiator and wave reflected from the metasurface superstrate, and due to the geometry of the proposed structure, the superstrate-loaded antenna provides directional radiation pattern. Because of the presence of metasurface superstrate, not only directional radiation pattern is observed, but 3-dB axial bandwidth is also improved (a rise of 1.29 times, i.e., 720 MHz to 930 MHz). The enhancement of 3-dB axial bandwidth is specifically due to the generation of strong orthogonal field components in the corresponding frequency bands.

Table 2. Effect of various antenna parameters and parametric study regarding placement of metasurface superstrate on the proposed antenna (stage-3).

$h_{\text{air-gap}}$	Impedance Bandwidth	Axial Bandwidth	CP Antenna Gain
30 mm	2.07–6.71 GHz, 106.9%	———	———
35 mm	1.99–6.74 GHz, 108.8%	———	———
40 mm	1.92–6.77 GHz, 111.6%	———	———
45 mm	1.81–6.88 GHz, 117.9%	4.07–5 GHz, 20.66%	6.78 dBic
50 mm	1.73–6.77 GHz, 118.5%	4.4–4.92 GHz, 11.15%	6.91 dBic
55 mm	1.46–6.78 GHz, 129.1%	4.48–4.5 GHz, 10.97%	6.89 dBic
60 mm	1.13–6.77 GHz, 142.7%	———	———

The gap ($h_{\text{air-gap}}$) between radiator and metasurface superstrate depends on the thickness of substrate (h_{sub}), relative permittivity of substrate (ε_r), and λ_0 (guided free-space wavelength at $f = 5$ GHz) as shown in Equation (4). With the consideration of Equation (6), $h_{\text{air-gap}}$ is 45.24 mm (theoretical) against $h_{\text{air-gap}}$ of 45 mm (simulated). Table 2 shows the understanding about variation of $h_{\text{air-gap}}$ and its relative impact on different antenna parameters such as impedance bandwidth, axial bandwidth, and CP antenna gain. The mathematical formulation given in Equation (4) can be applied to the case of any superstrates and reflectors in analyzing their placement ($h_{\text{air-gap}}$) with respect to the radiator.

$$h_{\text{air-gap}} = 0.76\lambda_0 - h_{\text{sub}}\sqrt{\epsilon_r} \tag{4}$$

The proposed metasurface antenna exhibits broad impedance bandwidth (1.81–6.88 GHz, 117.9%), broad axial bandwidth (4.07–5 GHz, 20.66%), and average CP antenna gain of 6.78 dBic with the average antenna directivity of 6.97 dBi. It exhibits better outcomes than the existing works reported in [7–19]. Thus, the objective of incorporating a metasurface as a superstrate is satisfied in this design process.

3. EVALUATION OF CP ATTRIBUTES IN TERMS OF AXIAL BANDWIDTH AND CP ANTENNA GAIN

To evaluate CP traits, theoretical insights regarding the analysis of CP antennas are presented in terms of axial bandwidth ($\text{BW}_{\text{3-dB}}$) and CP antenna gain ($G_{\text{3-dB}}$). The intuition behind proposed criteria (C_{r1}–C_{r4}) correlates with the analysis of CP antennas, applicable regardless of their geometry and frequency of operation. A detailed analogy about its mathematical derivation is highlighted from Equations (5) to (11). The outcomes with realization to various CP antennas reported in [11–19] are shown in Table 3. The CP characteristics are compared taking account of different parameters. These criteria are used for a more complete evaluation of antenna characteristics.

To understand such a phenomenon for the proposed metasurface antenna (stage-3) in our study, let us consider the criteria (C_r) including (a) 3-dB axial bandwidth ($\text{BW}_{\text{3-dB}}$) and (b) CP antenna gain ($G_{\text{3-dB}}$). For the analysis, it can be represented as a function of:

$$C_r = F(\text{BW}_{\text{3-dB}}, G_{\text{3-dB}}) \tag{5}$$

By considering product of 3-dB axial bandwidth and the CP antenna gain, C_r takes the form of:

$$C_r = \text{BW}_{\text{3-dB}} \times G_{\text{3-dB}} \tag{6}$$

Further, dividing the 3-dB axial bandwidth by 100, percentage representation of $\text{BW}_{\text{3-dB}}$ can be removed from the criteria measurement unit. Thus, the final form of C_r can be expressed as:

$$C_r = \frac{\text{BW}_{\text{3-dB}} \times G_{\text{3-dB}}}{100} \tag{7}$$

Equation (7) presents the basic form of the proposed criteria for analyzing CP characteristics. Here, it takes consideration of 3-dB axial bandwidth and CP antenna gain, often considered as the important

Table 3. Evaluation of CP antennas [11–19] in compliance with proposed criteria: C_{r1} and C_{r4}.

Ref.	Type of Antenna	$BW_{3\text{-dB}}$	$G_{3\text{-dB(avg)}}$	$G_{3\text{-dB(peak)}}$	C_{r1}	C_{r4}
[11]	Monopole	5.1%	4.1 dBic	4.1 dBic	0.21	0.21
[12]	Monopole	10%	5.5 dBic	6.67 dBic	0.55	0.66
[13]	Monopole	16.5%	5.8 dBic	5.8 dBic	0.95	0.95
[14]	Monopole	18.69%	5.1 dBic	6.1 dBic	0.95	1.14
[15]	Dipole	18%	4.8 dBic	6.8 dBic	0.86	1.22
[16]	DRA	10.6%	———	———	———	———
[17]	DRA	18.2%	> 4 dBic	4.3 dBic	0.72	0.78
[18]	DRA	11.57%	2.68 dBic	3.8 dBic	0.31	0.43
[19]	DRA	17.59%	3.86 dBic	4.2 dBic	0.67	0.73
Proposed	Monopole	20.02%	6.82 dBic	7.24 dBic	1.37	1.45

system parameters for an RF front-end in RF energy harvesting system [21]. These 4 proposed criteria can be used for the evaluation of CP antennas [Equations (8) to (11)] derived with the segregation of CP antenna gain and evaluated in the terms of (a) average (G_{avg}), (b) maximum ($G_{\max}$), (c) minimum ($G_{\min}$), and (d) peak (G_{peak}). The set of proposed criteria can be represented as:

$$C_{r1} = \frac{BW_{3\text{-dB}} \times G_{3\text{-dB(avg)}}}{100} \tag{8}$$

$$C_{r2} = \frac{BW_{3\text{-dB}} \times G_{3\text{-dB(max)}}}{100} \tag{9}$$

$$C_{r3} = \frac{BW_{3\text{-dB}} \times G_{3\text{-dB(min)}}}{100} \tag{10}$$

$$C_{r4} = \frac{BW_{3\text{-dB}} \times G_{3\text{-dB(peak)}}}{100} \tag{11}$$

C_{r1} and C_{r4} as the proposed criteria are evaluated with reference to proposed superstrate antenna and other existing antenna designs reported in [11–19]. By utilizing C_{r1}–C_{r4}, the complete evaluations of RF front-ends is possible. The above given theoretical insights are presented in a quite simplified manner and utilized directly, compared to [25], where there is no consideration of CP peak antenna gain, considered as one of the important system parameters in RF energy harvesting application [1, 20, 21]. Thus, an additional antenna parameter is investigated and reported, which strengthens the analysis for CP antennas. The intuition behind these proposed criteria relate with a complete evaluation of antenna characteristics, regardless of its nature/geometry and frequency of operation.

4. EXPERIMENTAL VALIDATION

The fabricated prototype of proposed metasurface antenna (stage-3), along with its measurement process is shown in Figure 4. The structural support of metasurface superstrate over circularly-shaped monopole radiator with asymmetrical staircased ground plane is taken care by the plastic spacers. The proposed metasurface antenna is fabricated by using a PCB-ETSMATE prototyping machine. The S_{11} parameter is measured by an Agilent N5247A PNA-X vector network analyzer (VNA) and far-field parameters such as axial ratio, antenna gain, and radiation pattern which are measured in an anechoic chamber. The measured impedance and axial bandwidth are 114.9% (1.85–6.85 GHz) and 20.02% (4.09–5 GHz), respectively, shown in Figure 5(a). Figure 5(b) shows simulated and measured antenna gains. The average simulated and measured gains are 6.78 dBic and 6.82 dBic, respectively, with simulated consistent antenna efficiency $> 85.65\%$ in the desired operating bands. Figures 6(a) and (b) present the measured far-field normalized radiation patterns at 4.5 GHz and 5 GHz. The metasurface

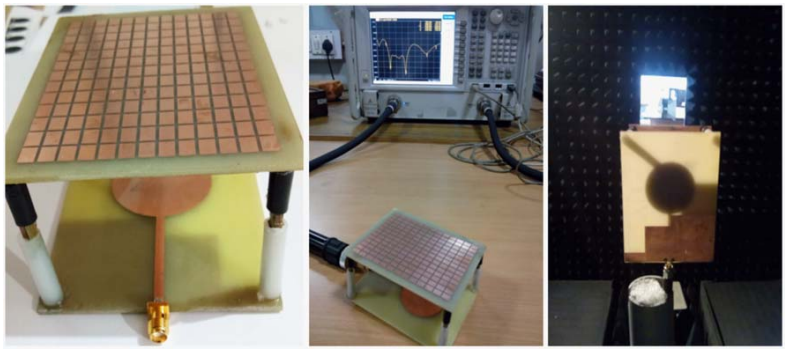

Figure 4. Fabricated prototype and experimental setup (including S_{11} measurement using VNA and far-field parameters measurement in an anechoic chamber) for the proposed metasurface antenna.

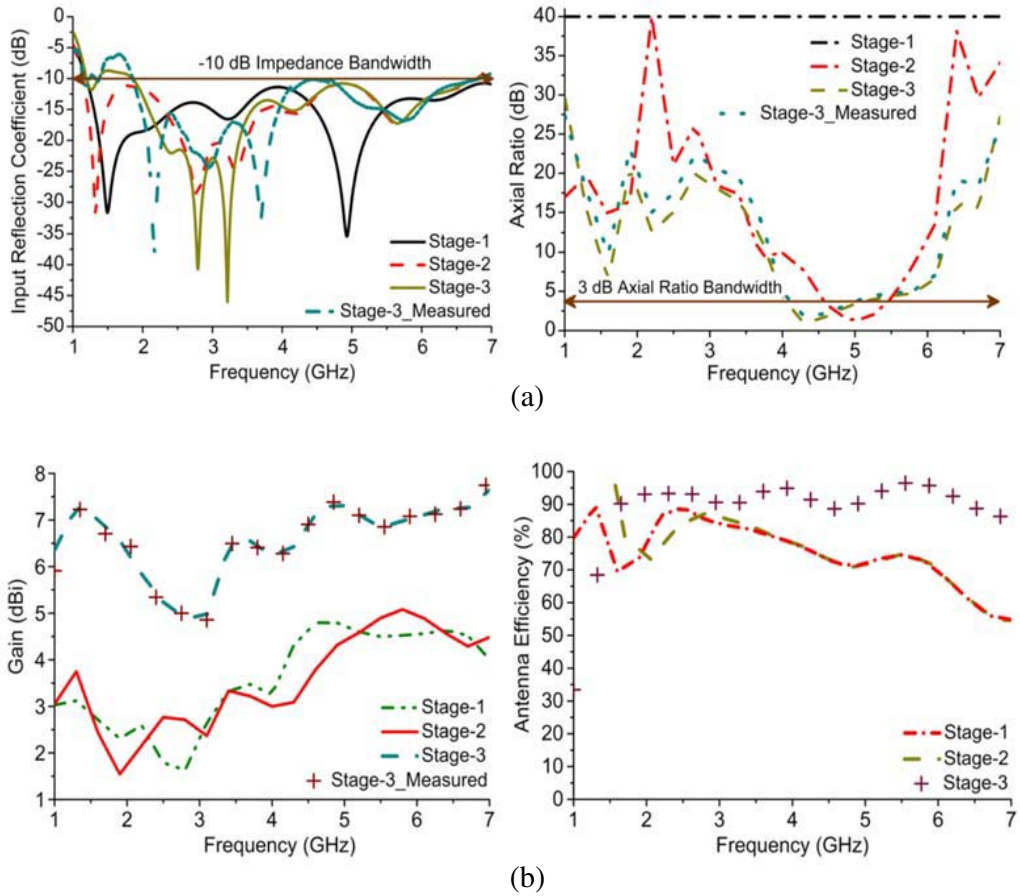

Figure 5. Simulated and measured (a) S_{11} and AR, (b) antenna gain (LP/CP); with simulated antenna efficiency from stage-1 to stage-3.

superstrate-inspired broadband CP printed monopole antenna offers a directional pattern with 3-dB angular beamwidth $> 100°$ in the broadside direction.

Table 4 highlights the performance metrics of different antenna parameters for stage-1 to stage-3. Among these three stages, stage-3 witnesses better performance compared with the existing antennas designs [7–19]. The proposed metasurface antenna excels over the referred instances in terms of broadband CP, enhanced CP antenna gain of $>$ 6.5 dBic, and antenna efficiency of $>$ 85.65% in

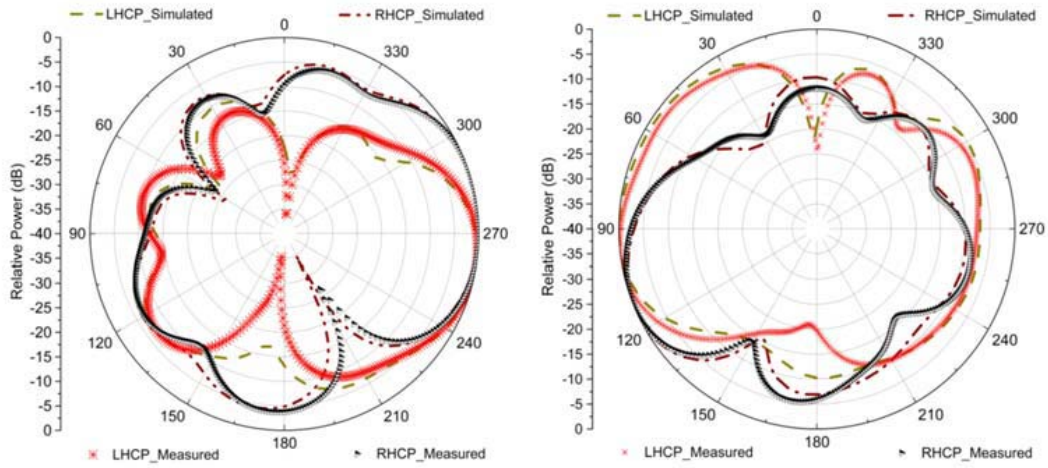

(a)

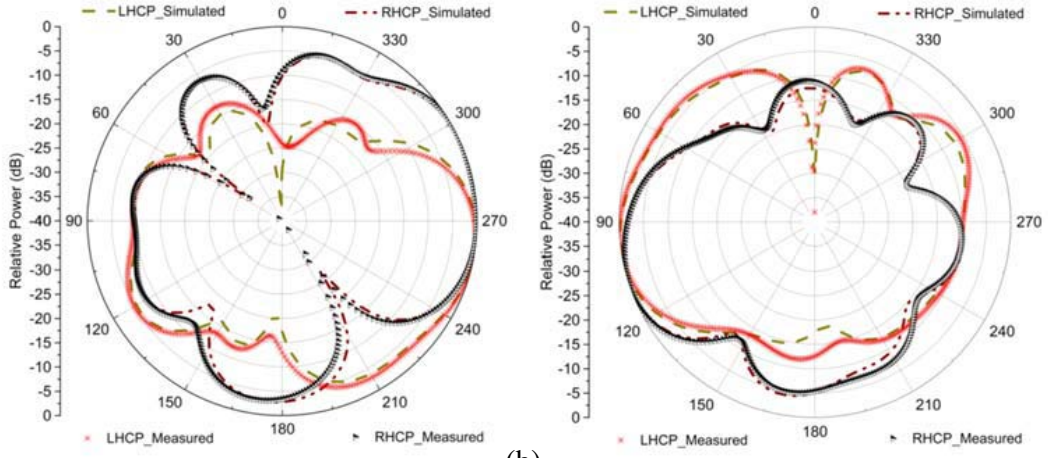

(b)

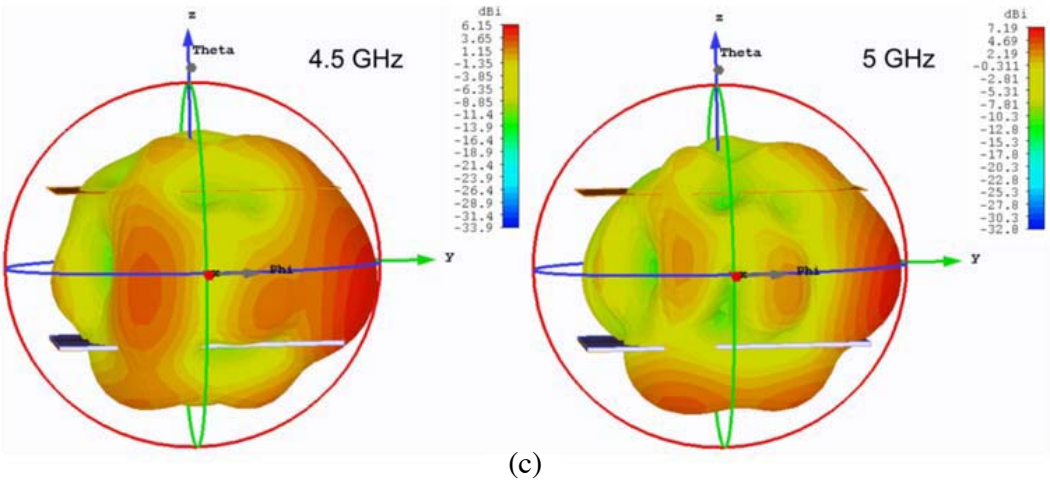

(c)

Figure 6. Simulated and measured normalized radiation pattern at (a) $f = 4.5\,\text{GHz}$, (b) $f = 5\,\text{GHz}$ and its (c) 3D pattern of dominated component of the metasurface superstrate inspired monopole antenna.

Table 4. A comparison of performance index [stage-1 to 3] of the proposed antenna configurations.

Antenna Parameters	Stage-1	Stage-2	Stage-3	Stage-3
Execution (Nature)-I	Initial	LP-to-CP	Final Stage	Final Stage
Execution (Nature)-II	Simulated	Simulated	Simulated	Measured
S_{11}	1.2–7.2 GHz	1.1–6.8 GHz	1.81–6.88 GHz	1.85–6.85 GHz
Impedance Bandwidth-I	6 GHz	5.7 GHz	5.07 GHz	5 GHz
Impedance Bandwidth-II	142.8%	144.3%	117.9%	114.9%
Axial Ratio (AR)	———	4.65–5.37 GHz	4.07–5 GHz	4.09–5 GHz
Axial Ratio Bandwidth-I	———	720 MHz	930 MHz	910 MHz
Axial Ratio Bandwidth-II	———	14.1%	20.66%	20.02%
Antenna Gain	3.4 dBi	2.3 dBic	6.78 dBic	6.82 dBic
Antenna Directivity	5.89 dBi	6.07 dBi	6.97 dBi	———
Antenna Efficiency	$> 70\%$	$> 70\%$	$> 85.65\%$	———
3-dB Angular Beamwidth	———	76.8°	$> 100°$	$> 100°$
Radiation Pattern	Omni-Directional	Omni-Directional	Directional	Directional

the desired frequency bands. It also offers the characteristics of low-profile, easy implementation and portability, which is significant for RF energy harvesting [1, 20, 21].

Due to the incorporation of metasurface superstrate, a directional pattern is observed in the broadside direction shown in Figure 6. Such type of radiation properties is different from a conventional printed monopole antenna. Conventional printed monopole antennas exhibit only omnidirectional characteristics [4]. Being the traditional directional antenna, it holds certain advantage such as possibility of lower interference, improved spatial reuse, longer transmission range, and reduced power requirement. Substantially, the antennas with omnidirectional radiation cause path loss with increasing transmission distance, due to the beam spreading, often compensated by utilizing directional antennas.

These outcomes also present a picture that the proposed metasurface antenna is a generic solution in achieving trade-offs (broadband CP, enhanced CP antenna gain, consistent antenna efficiency, etc.), especially metasurface enabled radiators reported in recent period-of-times [24, 26–28]. Table 5 highlights the comparison of performance metrics with that of the proposed metasurface antenna.

Table 5. A comparison of existing metasurface enabled radiators in the same field of interest reported in [24, 26–28].

Ref./ Year	Type of Antenna	Impedance Bandwidth	Axial Bandwidth	CP Antenna Gain	Time Domain Analysis	RF Energy Harvesting
24/2015	Printed	28%	———	———	———	———
26/2017	Printed	30%	———	———	———	———
27/2019	Printed	67.3%	———	———	———	———
28/2020	Printed	29.41%	9.05%	6.34 dBic	———	———
Proposed	Printed	114.9%	20.02%	6.82 dBic	Investigated	Investigated

5. TIME DOMAIN ANALYSIS

Time domain analysis is important for broadband antennas [4], which describes the signal transmission and its reception capabilities with minimum distortion, as a fundamental entity. The antenna parameters such as group delay and isolation are analysed over the desired operating bands. CST microwave studio

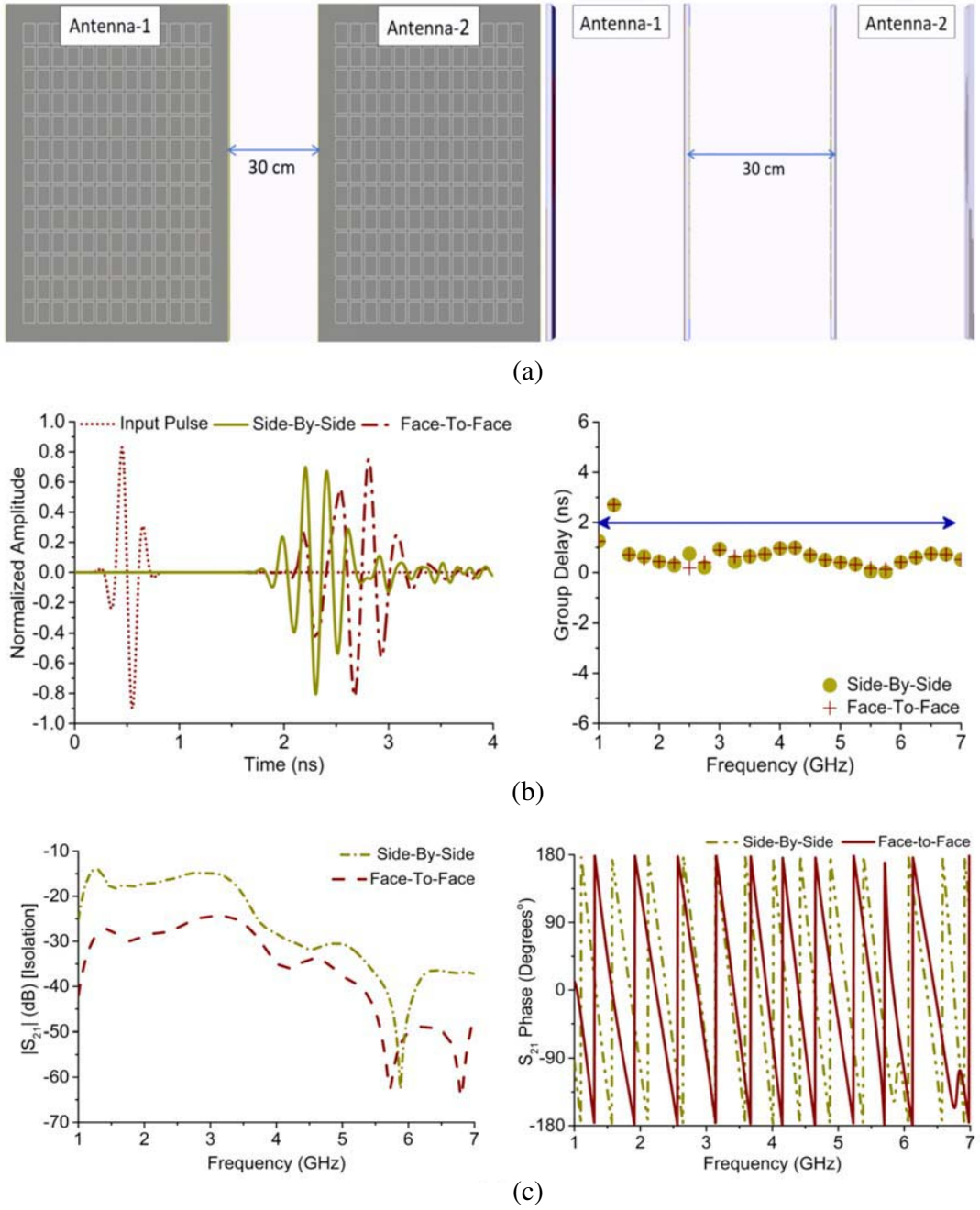

Figure 7. Evaluation of time domain analysis of the proposed metasurface antenna (a) side-by-side and face-to-face arrangements, (b) normalized input & output pulse and variation in group delay (in terms of ns), (c) variation of isolation (in terms of dB) and variation of S_{21} phase (in terms of degrees).

is used to pursue the time domain analysis. The identical radiating structures of proposed metasurface antenna are kept at (a) side-by-side and (b) face-to-face arrangements, with the intermediate distance of 30 cm in between them. The monopole radiator is characterized in the broadside direction, for showing a better prospective in terms of antenna performance. A detailed analysis, along with its corresponding outcomes, is shown in Figures 7(a)–(c).

A Gaussian pulse is used for analyzing the characteristics of its signal behaviour. It is observed from these outcomes that with better isolation (dB) and approximately linear phase variation, metasurface

antenna demonstrates good pulse handling capability, as demanded by communication systems. In the literature, RF front-end is considered an integral part of an RF energy harvesting system, which predominantly receives RF signals emitted from other ambient sources. Since the RF energy that is available in the surrounding environment can exist in any orientation and phase alignment, CP antennas in the broadside direction with enhanced CP antenna gain are more desirable for RF energy harvesting systems. Output traits of the proposed antenna derived from time domain analysis can be correlated with the indoor measurement of rectenna system, which is related to the Friis Transmission Equation [1].

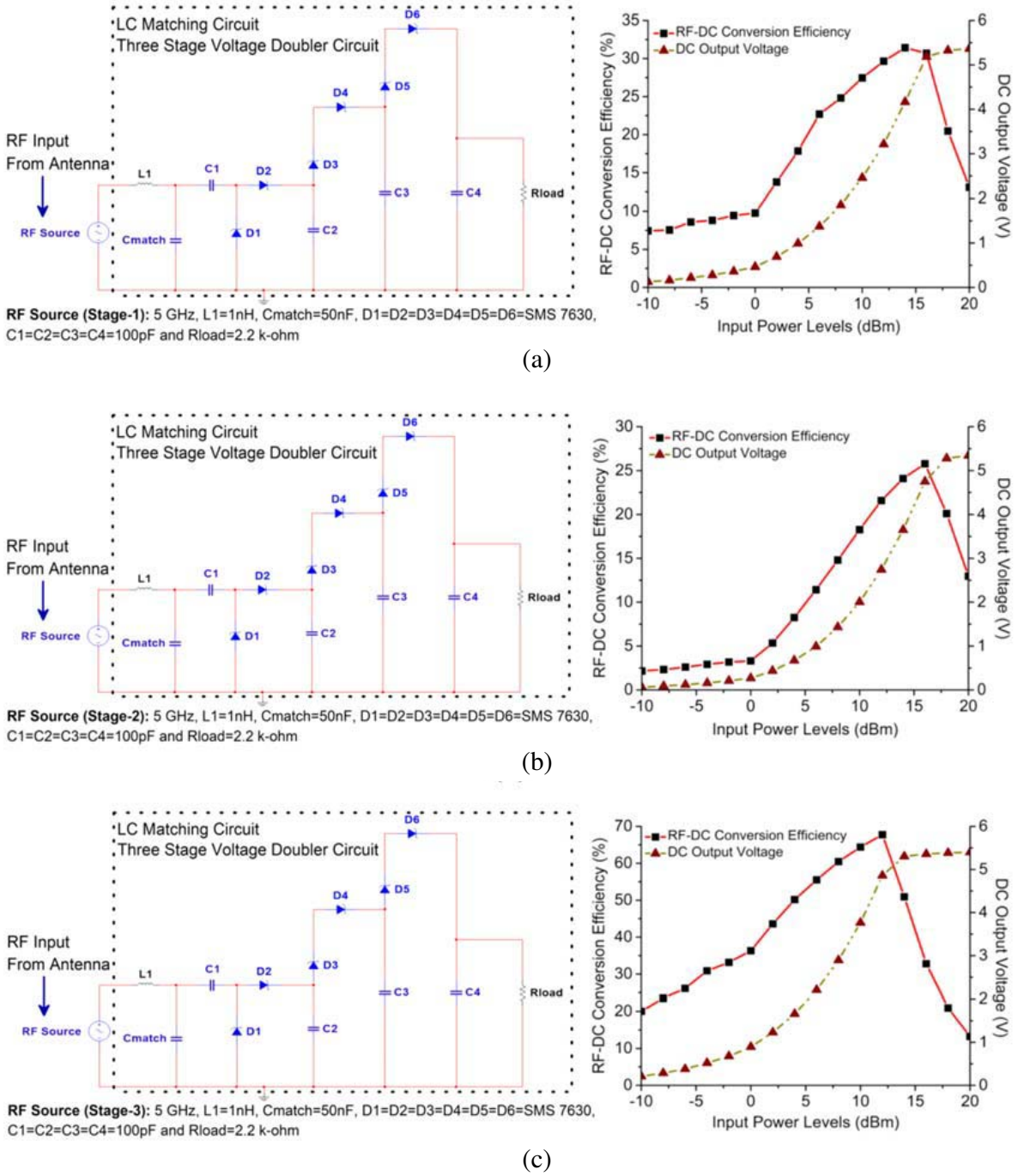

Figure 8. Circuit diagram and RF-to-DC conversion efficiency of rectifier circuit embedded with the proposed antenna configurations (a) stage-1 (initial), (b) stage-2 and (c) stage-3 (final).

6. IMPLEMENTATION OF DESIGNED RECTIFIER CIRCUIT

The proposed metasurface antenna is integrated with a rectifier circuit consisting of L-C matching network and Greinacher voltage doubler (GVD) for RF energy harvesting application. To bring more intuition behind the metasurface antenna, performance levels of individual antenna configurations (stage-1 to 3) have been investigated and shown in Figures 8(a)–(c). The parameters such as RF-to-DC conversion efficiency (η_0) are calculated by considering the topology of Equation (14), and DC output voltage (V_{out}) is taken through the evaluation of circuit variables at the ADS platform.

$$\eta_0(\%) = \frac{P_{\text{load}}}{P_{\text{incident}}} = \frac{V_{\text{out}}^2}{P_{\text{in}} \times R_{\text{load}}} \tag{12}$$

In our study, the designed rectifier circuit is analysed for input power levels (P_{in}), from -10 to 20 dBm. On interpretation of the circuit variables in a test environment at ADS, with a load resistance (R_{load}) of 2.2 kΩ, V_{out} is 3.21 V with η_0 calculated as 29.7% at 12 dBm (for stage-1); V_{out} is 2.73 V with η_0 calculated as 21.6% at 12 dBm (for stage-2); and V_{out} is 4.86 V with η_0 calculated as 67.8% at 12 dBm (for stage-3). Prior to simulation, theoretical insights about the proposed rectifier model are also investigated. Here, each individual stage with its dedicated GVD configuration is considered as the single battery having open circuit output voltage ($V_{\text{o.c.}}$), internal resistance (R_{int}), and load resistance (R_{load}). Henceforth, the output voltage (V_{out}) can be expressed as:

$$V_{\text{out}} = \frac{V_{\text{o.c.}}}{R_{\text{int}} + R_{\text{load}}} \times R_{\text{load}} \tag{13}$$

For n number of stages in series and connected to R_{load}, V_{out} can be represented as:

$$V_{\text{out}} = \frac{nV_{\text{o.c.}}}{nR_{\text{int}} + R_{\text{load}}} \times R_{\text{load}} \tag{14}$$

Thus, the number of stages in the system has a significant effect on the output voltage (V_{out}) [29], which can be referenced from Equations (15) and (16). The realization of such high amount of DC harvested voltage lies in the usage of partial ground plane in the proposed metasurface antenna, resulting in maximizing the captured energy, which can energize the sensors in internet-of-things (IoTs) application. Continuing in our investigation, the utilization of metasurface [20, 21, 30] is used to enhance gain and directivity of RF front-end. Inan RF energy harvesting system, the received power is one of the important parameters that evaluate the performance of rectenna model. With the specific conditions of operating frequency and availability of ambient RF signals, enhanced CP antenna gain is the only possible way-out to maximize the outcomes of RF energy harvesting, as interpreted from Table 6 and Figures 8(a)–(c).

Table 6. The performance metrics of individual antenna configurations (stage-1 to 3) after integrating rectifier circuit in the test environment of ADS platform at $f = 5$ GHz [i.e., Wi-Fi (5 GHz), Wi-MAX (5 GHz), ISM (5 GHz) and 5G (5 GHz)].

Geometrical Sequences	Antenna Gain (LP/CP)	Input Power Levels	DC Output	η_0
Stage-1 (Initial)	3.4 dBi (LP)	12 dBm	3.21 V	29.7%
Stage-2 (Intermediate)	2.3 dBic (CP)	12 dBm	2.73 V	21.6%
Stage-3 (Final)	6.78 dBic (CP)	12 dBm	4.86 V	67.8%

7. CONCLUSION

A metasurface superstrate-based broadband CP printed monopole antenna with directional pattern have been presented and studied. It exhibits broadened impedance & axial bandwidth, average measured CP gain of 6.82 dBic, and antenna efficiency $> 85.65\%$ in the operating bands. Besides simulation and characterization, a detailed explanation about attainment of broadband CP, backed by surface current

distribution, electric field distribution & normalized far-field radiation and directional radiation pattern characteristics in broadside direction, with incorporation of metasurface superstrate is investigated. The obtained outcomes suggest that it can be an excellent candidate for RF energy harvesting. Therefore, the proposed metasurface antenna is integrated with a designed rectifier circuit, where the parameters such as RF-to-DC conversion efficiency (η_0) and DC output voltage (V_{out}) are analyzed by using ADS platform. It shows better performance ($\eta_0 = 67.8\%$ and $V_{\text{out}} = 4.86\,\text{V}$ at $12\,\text{dBm}$) than other antenna configurations, reported in Table 6.

REFERENCES

1. Behera, B. R., P. R. Meher, and S. K. Mishra, "Microwave antennas — An intrinsic part of RF energy harvesting systems: A contingent study about its design methodologies and state-of-art technologies in current scenario," *International Journal of RF and Microwave Computer-Aided Engineering*, Vol. 30, No. 5, e22148, 1–27, 2020.
2. Maybell, M. J., "A polarization basics diagram," *IEEE Antennas and Propagation Magazine*, Vol. 61, No. 1, 130–135, 2019.
3. Toh, B. Y., R. Cahill, and V. F. Fusco, "Understanding and measuring circular polarization," *IEEE Transactions on Education*, Vol. 46, No. 3, 313–318, 2003.
4. Mishra, S. K., et al., "A compact dual-band fork-shaped monopole antenna for Bluetooth and UWB applications," *IEEE Antennas and Wireless Propagation Letters*, Vol. 10, 627–630, 2011.
5. Liang, J., et al., "Study of a printed circular disc monopole antenna for UWB systems," *IEEE Transactions on Antennas and Propagation*, Vol. 53, No. 11, 3500–3504, 2005.
6. Pandey, R., A. K. Shankhwar, and A. Singh, "Design, analysis, and optimization of dual side printed multiband antenna for RF energy harvesting applications," *Progress In Electromagnetics Research C*, Vol. 102, 79–91, 2020.
7. Mathur, M., A. Agrawal, G. Singh, and S. K. Bhatnagar, "A compact coplanar waveguide fed wideband monopole antenna for RF energy harvesting applications," *Progress In Electromagnetics Research M*, Vol. 63, 175–184, 2018.
8. Dastranj, A., "Very small planar broadband monopole antenna with hybrid trapezoidal-elliptical radiator," *IET Microwaves, Antennas & Propagation*, Vol. 61, No. 4, 542–547, 2017.
9. Elsheakh, D. M. and E. A. Abdallah, "Ultra-wide-bandwidth (UWB) microstrip monopole antenna using split ring resonator (SRR) structure," *International Journal of Microwave and Wireless Technologies*, Vol. 10, No. 1, 123–132, 2018.
10. Ray, K. P. and Y. Ranga, "Ultrawideband printed elliptical monopole antennas," *IEEE Transactions on Antennas and Propagation*, Vol. 55, No. 4, 1189–1192, 2007.
11. Ghosh, S. and A. Chakrabarty, "Dual band circularly polarized monopole antenna design for RF energy harvesting," *IETE Journal of Research*, Vol. 62, No. 1, 9–16, 2016.
12. Yue, T., Z. H. Jiang, and D. H. Werner, "Compact, wideband antennas enabled by interdigitated capacitor-loaded metasurfaces," *IEEE Transactions on Antennas and Propagation*, Vol. 64, No. 5, 1595–1606, 2016.
13. Wu, Z., et al., "Metasurface superstrate antenna with wideband circular polarization for satellite communication application," *IEEE Antennas and Wireless Propagation Letters*, Vol. 15, 374–377, 2016.
14. Chen, Q., et al., "Wideband and low axial ratio circularly polarized antenna using AMC-based structure polarization rotation reflective surface," *International Journal of Microwave and Wireless Technologies*, Vol. 10, No. 9, 1058–1064, 2018.
15. Yang, W., et al., "Novel polarization rotation technique based on an artificial magnetic conductor and its application in a low-profile circular polarization antenna," *IEEE Transactions on Antennas and Propagation*, Vol. 62, No. 12, 6206–6216, 2014.
16. Chair, R., et al., "Aperture fed wideband circularly polarized rectangular stair shaped dielectric resonator antenna," *IEEE Transactions on Antennas and Propagation*, Vol. 54, No. 4, 1350–1352, 2006.

17. Wang, K. X. and H. Wong, "A circularly polarized antenna by using rotated-stair dielectric resonator," *IEEE Antennas and Wireless Propagation Letters*, Vol. 14, 787–790, 2015.
18. Altaf, A., et al., "Circularly polarized spidron fractal dielectric resonator antenna," *IEEE Antennas and Wireless Propagation Letters*, Vol. 14, 1806–1809, 2015.
19. Kumar, R., S. R. Thummaluru, and R. K. Chaudhary, "Improvements in Wi-MAX reception: A new dual-mode wideband circularly polarized dielectric resonator antenna," *IEEE Antennas and Propagation Magazine*, Vol. 61, No. 1, 41–49, 2019.
20. Divakaran, S. K., D. D. Krishna, and Nasimuddin, "RF energy harvesting systems: An overview and design issues," *International Journal of RF and Microwave Computer-Aided Engineering*, Vol. 29, No. 1, e21633, 1–15, 2019.
21. Wagih, M., A. S. Weddell, and S. Beeby, "Rectennas for radio-frequency energy harvesting and wireless power transfer: A review of antenna design," *IEEE Antennas and Propagation Magazine*, Vol. 62, No. 5, 95–107, 2020.
22. Behera, B. R., et al., "A compact broadband circularly polarized printed monopole antenna using twin parasitic conducting strips and rectangular metasurface for RF energy harvesting application," *AEÜ-International Journal of Electronics and Communications*, Vol. 120, 15233, 1–10, 2020.
23. Harrington, R. F., *Time-harmonic Electromagnetic Fields*, Wiley-IEEE Press, New York, USA, 2001.
24. Liu, W., Z. N. Chen, and X. M. Qing, "Metamaterial-based low-profile broadband aperture-coupled grid-slotted patch antenna," *IEEE Transactions on Antennas and Propagation*, Vol. 63, No. 7, 3325–3329, 2015.
25. Kirov, G. S., "Evaluation of the frequency bandwidth and gain properties of antennas: Characteristics of circularly polarized microstrip antennas," *IEEE Antennas and Propagation Magazine*, Vol. 62, No. 3, 74–82, 2020.
26. Liu, W. E. I., et al., "Miniaturized wideband metasurface antennas," *IEEE Transactions on Antennas and Propagation*, Vol. 65, No. 12, 7345–7349, 2017.
27. Wang, J., et al., "Broadband CPW-fed aperture coupled metasurface antenna," *IEEE Antennas and Wireless Propagation Letters*, Vol. 18, No. 3, 517–520, 2019.
28. Rajanna, P. K., K. Rudramuni, and K. Kandasamy, "Characteristic mode-based compact circularly polarized metasurface antenna for in-band RCS reduction," *International Journal of Microwave and Wireless Technologies*, Vol. 12, No. 2, 131–137, 2020.
29. Din, N. M., C. K. Chakrabarty, A. Bin Ismail, K. K. A. Devi, and W.-Y. Chen, "Design of RF energy harvesting system for energizing low power devices," *Progress In Electromagnetics Research*, Vol. 132, 49–69, 2012.
30. Liu, R., et al., "Metasurface: Enhancing gain of antenna and energy harvesting system design," *International Journal of RF and Microwave Computer-Aided Engineering*, Vol. 30, No. 2, e22053, 1–11, 2020.